1-1-2008

MEMS Transducer for Hearing Aid Device

Houwen Tang
University of Denver

MEMS TRANSDUCER FOR HEARING AIDS

_____

A Thesis

Presented to

the Faculty of Engineering and Computer Science

University of Denver

_____

In Partial Fulfillment

of the Requirements for the Degree

Master of Engineering

_____

by

Houwen Tang

November 2008

Advisor: M.A. Matin and Yunbo Yi

Author: Houwen Tang
Title: MEMS Transducer for hearing aids
Advisor: M. A. Matin and Yunbo Yi
Degree Date: November 7, 2008

ABSTRACT

An implantable MEMS piezoelectric transducer for middle ear hearing aids was developed. The physical vibration properties are simulated using finite element method. A study of thermoelastic damping effect of four designed MEMS mirrors is presented. An optical measurement system based on Mach-Zehnder interferometer is developed, and the accuracy of this system is tested.

ACKNOWLEDGMENTS

I would like to thank my advisors, Dr. Mohammad Matin and Dr. Yunbo Yi. Dr. Yi was the first mentor to lead me to the world of MEMS and Dr. Matin opened my eyes to the optoelectronics field and influenced me with his own hard work. I would not have the practical capability without their help. I would like to thank both of them for their advise and encouragement.

Table of Contents

LIST OF TABLES

LIST OF FIGURES

CHAPTER 1

INTRODUCTION

Micro-electro-mechanical system, usually referred to MEMS, is a technique used to fabricate devices and machines in micro-scale. It integrates a number of micro-components, including microelectronic integrated circuits, sensors, and actuators on a single chip that allows the micro-system to both sense and control the environment.

MEMS applications are all around our everyday life. For example: vibration sensors for load imbalance used in washing machines, accelerometers, ABS used in cars, the dirt sensors used in vacuums, the strain gages for food weight used in microwave ovens, etc. MEMS technology is definitely part of a revolution that is expanding the future of possible designs and applications [Ref.1].

In the past few years, there has been a growing interest in MEMS hearing aids [Ref.2]. The primary motivation for this research was its potential use in application, which was not accessible to conventional, outers-ear wearing air-gap electromagnetic hearing devices. First of all, Implantable hearing aids directly transfer sound signals into vibration energy, which drives the ear. In other words, steps that degrade the signal are taken away. Another principal advantage for Implantable piezoelectric hearing aids is that they are largely more efficient in power and in size. Also, the piezoelectric transducer requires less power consumption, and it has more compatibility with the external magnetic environment [Ref.3]. Other possible advantages of piezoelectric transducers are that they are very reliable and inexpensive because they convert electrical signals into physical motion. It has also been proven that the piezoelectric transducer exhibits a high tolerance to environmental factors

such as electromagnetic fields and humidity [Ref.4]. These characteristics of piezoelectric transducer can bring down the cost for conventional electromagnetic hearing aids and offer an even more natural sound

In order to make such MEMS piezoelectric transducers acceptable in real life applications, researchers have to solve several problems. These include low sensitivity, feedback noise, unstable device characteristics, high cost of components and fabrication conditions.

This thesis presents the principles involved in a designed implantable middle-ear piezoelectric transducers for hearing aids, as well as a simulation and detailed characterization. First, we examine the basic mechanical properties of PZT-5H. Further, we proposed a PZT-5H based piezoelectric transducer with its base made of SiO_2 and PZT-5H sandwiched by two layers of Aluminum. The geometry effect of each component is fully investigated under a certain loading condition. By discretizing the device, finite element method is applied to evaluate the vibrating deflection at the tip of this device.

In addition to that, we are also very interested in the damping effect of our design, especially the thermoelastic damping effect. Since it is known that thermoelastic damping is significantly crucial to the MEMS resonators, we extended our study to MEMS mirrors used as MEMS resonators. We presented four different designs of MEMS mirrors, and a comparison of each model's quality factors is discussed with different geometries. The simulation result is found to be of great help, and address the energy concern of MEMS mirrors used as resonators.

Lastly, we developed a frequency measurement system since we are looking forward to fabricating this device and comparing our simulation data with experimental result in the near future. This optical system is based on Mach-Zehnder

interferometer and we tested our system with some practical data. We will be using this system to obtain some physical vibration properties of our device.

Our future work will be focusing on fabricating implantable MEMS piezoelectric transducer using MEMS technologies. And due to the rapid improvement of digital technology and feedback cancellation, we are looking forward to bring digital signal processing for future innovation of current hearing aids.

CHAPTER 2

PIEZOELECTRIC TRANSDUCER

This chapter presents the fundamentals of our MEMS piezoelectric transducer, including basic structures, physical principles and material properties. Finite element method is applied for our simulation.

2.1 Introduction

2.1.1 Hearing aids

A hearing aid device is an electro-acoustic body-worn apparatus that can amplify and modulate sounds for the wearer. It first came into use at the beginning of the 1900s. At that time, people used a large vacuum tube to amplify the sound. Later on, Raytheon developed miniature vacuum tubes and made body-worn hearing aids a reality. However, the power consumption of these tubes requires large batteries, which made it hard for the user to carry such a large device. With the rapid development of science and technology in the 1950s, hearing aids were greatly improved in all aspects. One of the most significant upgrades was the replacement of large-scale tubes with transistors. Transistors hearing aids, also known as electronic hearing aids, only need one battery for its power supply [Ref.5]. The reduced size allowed the development of new types of hearing aid. Since then, all kinds of hearing aids, such as Behind-the-ear aids (BTE), In-the-ear aids (ITE), In-the-canal aids (ITC) were invented. Those devices have smaller sizes and better performances compared to the vacuum tube hearing aids. ITC for instance, is designed for mild to moderately severe hearing loss people and it can fit into the ear canal instead of needing to be placed on the ear. Since the microphone is placed in the ear canal, it offers natural sound reception. MEMS

hearing aids are were designed in micro-scale and implantable hearing aids are becoming popular because of their reliable performance and natural sound with less feedback distortion [Ref.6].

No matter which kind of hearing aid people are using, the device has four basic components: a power supply, a microphone, an amplifier and a receiver. The microphone is basically a transducer that can convert the sound signal into electrical energy. The amplifier, which is generally composed of transistors that are built into an integrated circuit, is used to amplify the electrical signal from the microphone. The receiver receives the amplified signal and transforms the modified electrical signal back to sound energy.

As one of the most major components of a hearing aid, the transducer, basically a microphone, plays a key role for providing a quality performance. There are two fundamental transducer designs available for hearing aids applications: the magnetic air-gap transducer and the piezoelectric transducer [Ref.7].

Currently, in the market, the most widely used transducer in hearing aid devices is the magnetic air-gap hearing transducer. An air-gap magnetic transducer converts acoustical energy into an electrical signal using a MEMS realization of capacitive microphone. The electrical signal is processed to drive a MEMS electromagnetic actuator. The resultant electromagnetic force generates a force on the micromagnet that has been implanted in the human ear. This technique has the superiority of low cost fabrication. However, they have a few shortcomings. As Sherif and Hamed have pointed out that though the air-gap capacitors have acceptable performance, they suffer from a fabrication complexity in forming the narrow air gap between relatively large surfaces [Ref.8]. They also suggested that the piezoelectric transducer, which is based on piezoelectric materials, do not need an air gap, which makes fabrication

process much easier than air-gap capacitors microphones, and the deflection can be directly measured. Further, piezoelectric ceramic can be cut in various ways to meet the requirements of different wave modes. Researchers believe that although there was a period in time when magnetic transducer dominates the acoustic hearing aids, the pendulum has now swung back toward piezoelectric materials.

A lot of new materials are being investigated before they can be used for certain applications, such as piezo-polymers and composites. Scientists also believe that the technology development of piezoelectric material has reached a point where it can be applied to all kinds of applications and replace some conventional devices, those in which sensors and actuators are essential to the functionality of the device.

Table 1: Piezoelectric Microphone vs. Air-gap magnetic Microphone

	Piezoelectric Microphone	Air-gap Magnetic Microphone
Sensitivity	Low	Good
Power Consumption	Low	High
Fabrication	Simple	Complicated
Dynamic Range	Wide	Narrow

2.1.2 Piezoelectricity

Piezoelectric material can be explained as some atomic lattice structures that have an essential cell a cubic or rhomboid atomic cage, and this cage holds a semi-mobile ion that has several stable quantum position states inside it [Ref.9]. It has the ability to generate an electric potential in response to an applied mechanical stress. The piezoelectric effect is also reversible, which means an applied voltage will change the shape of the material by a small amount. In physics, the piezoelectric effect can be defined as the link between electrostatics and mechanics.

The Pierre Curie brothers first discovered piezoelectric effect. They demonstrated the piezoelectricity effect using crystals such as quartz. Their work showed that the voltage is proportional to the mechanical stress applied on the crystals.

Piezoelectric materials can be divided in two main groups: crystals and ceramics. Most crystal piezoelectric materials are naturally occurring crystals, for example, berlintie ($AlPO_4$) and quartz (SiO_2). There are also some man-made crystals, such as gallium orthophosphate ($GaPO_4$) and Langasite ($La_3Ga_5SiO_{14}$). Ceramics are the other man-made piezoelectric materials available, for instance, barium titanate ($BaTiO_3$), which was the first piezoelectric ceramic discovered, and lead zirconate titanate (PZT), which is the most common piezoelectric ceramic in use today. Commercially, piezoelectric materials are not used in their pure forms. It is usually doped to satisfy different needs. Different dopants can change the piezoelectric characteristics as well as the physical properties of the material. Acceptor dopants are generally used to create oxygen (anion) vacancies and thus can harden the PZT [Ref.10]. Controversies to acceptor dopants, donor dopants are used to create metal vacancies and facilitate domain wall motion in the material to soft the PZT material. A list of the properties

for most common PZT material is demonstrated in Table 2.

Lately, it has been proved that lead zirconate titanate (PZT), which is a ceramic material made of lead (Pb), oxygen (O) and titanium (Ti) or zirconium (Zr), has the best piezoelectric properties, and it completely replaced the old day's barium titanate, which belongs to the group of electrical ceramics made of an oxide of barium and titanium. It also overcomes the shortcoming of inherently fragile of piezoelectric materials. These strong properties promised the lead zirconate titanate to be the dominant material for transducers. More and more researches have discovered new piezoelectric materials with better performance. For example, recent study of polyvinylidene fluoride (PVDF) showed that this material exhibits piezoelectricity several times greater than quartz, and other [Ref.11]. However, the study of this new material is not mature enough to put it into commercial use since the cost will be pretty high and the material is instable in some circumstances.

Table 2: Basic material property for commonly used PZT

Model	Piezo charge constants (pC/N)		Piezoelectric voltage constants (10^{-3}Vm/N)		Dielectric Constants	Youngs modulus (10^{10} N/m)		Density (10^3 kg/m^3)
	d_{33}	d_{31}	g_{33}	g_{31}	$\varepsilon T_{33}/\varepsilon_0$	YE_{11}	YE_{33}	ρ
PZT-4D	360	-145	31.7	-12.8	1280	7.5	6.2	7.7
PZT-8	280	-105	31	-11.9	1000	8.6	7.1	7.7
PZT-5A	450	-175	27	-11	1800	7.4	5	7.6
PZT-5B	460	-210	24.5	-10	2300	7.4	5	7.7
PZT-5J	550	-210	22.5	-8	2800	6.8	5	7.7
PZT-5H	640	-283	21	-9.3	3400	6	4.3	7.6
PZT-5X	750	-320	19	-8.2	4500	6.1	4.3	7.4

It has also been pointed out that the transducer has different properties for different uses. When the transducer is used a transmitter or a receiver, for its sensitivity requirements, it only permits a small defects proportional to the product of the efficiency of the transducer. On the other hand, when the transducer is used as a resolution, requires the transducer to perform high damp in order to locate defects near the surface. By doping PZT material, the hardness or softness of the material can be easily modified to meet all these specific requirements. This great character promises the PZT material will have a bright future that fits into all kinds of new designs and devices.

Many other factors, besides the material properties, may largely influence the behavior of a transducer, including the load conditions, the structure and construction, and even the damping effect. Thermoelastic damping, for instance, could largely affect the performance of a hearing aid, especially when the device scale shrinks to micro-scale and it is vibrating at a high frequency. The transducer could suffer from a high-energy loss due the instability of the heat transfer. As a consequence, the nature sound is distorted. The quality factor is generally used in physics and engineering to describe this type of damping.

Piezoelectric materials are now widely used in all kinds of fields, such as high voltage sources, sensors, actuators and motors, etc. An everyday life application example is the airbag sensor in the car. Piezoelectric material is used to detect the intensity of the shock and sends an electrical signal, which triggers the airbag.

2.1.3 Middle-ear Implantable MEMS piezoelectric transducer

Recently, the implantable MEMS piezoelectric transducer brings more and more interest due to its reliable performance. Several transducers have been developed for

middle ear or inner ear implant or semi-implant. Each design serves for a particular type of hearing loss.

In a normal person’s middle ear canal, there are three basic ossicles: malleus, incus, and stapes. The manubrium of the malleus attaches to the tympanic membrane, and was articulates to the incus at one end. The incus normally couples the sound energy from the eardrum to the stapes. The stapes is disposed in and against oval window of the cochlea. Some people may suffer from an ossicular lacking sufficient resiliency to transmit mechanical vibrations between the tympanic membrane and the oval window, to solve this issue, implantable middle ear hearing aids is needed for those patients.

Compared to other types of implantable hearing aids, piezoelectric hearing aid is advantageous for its simple structure and it provides a natural sound without and feedback distortion, which usually happens in an air-gap magnetic hearing aids.

Figure 1: Bones and muscles in the tympanic cavity in the middle ear

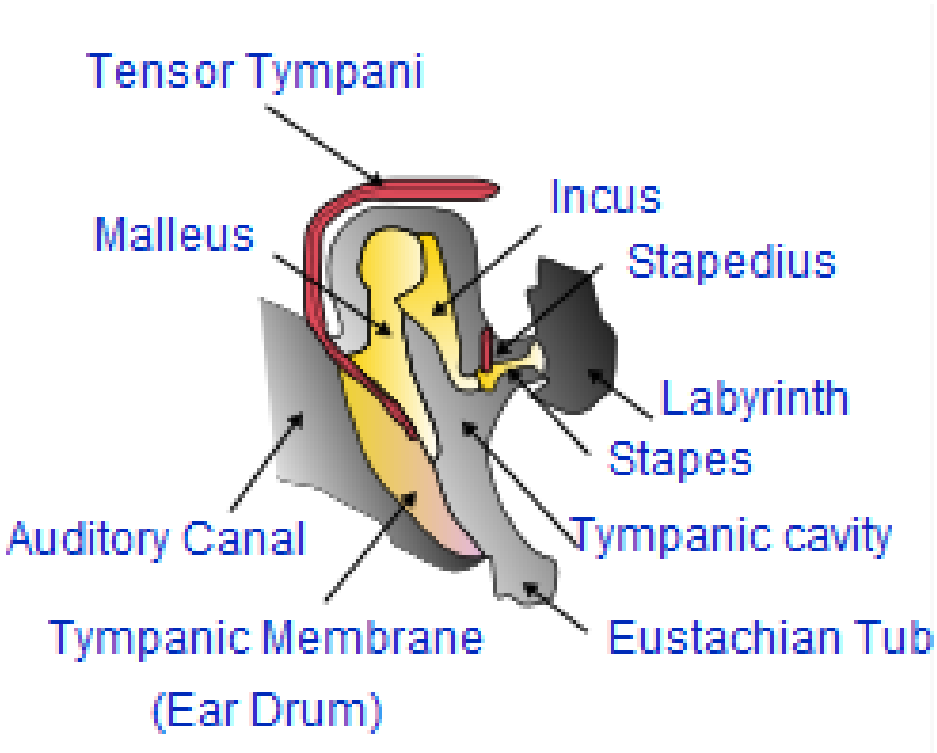

However, the sensitivity had always been an obstacle for it to become the dominant transducer for commercial purposes for a long time. Much research had been done to improve the performance of piezoelectric transducer. Several clamped-clamped transducers were proposed but they cannot improve their sensitivity greatly because of the residual stress in the diaphragm clamped on edges. However, in 1996, Seung S. Lee made a breakthrough design of a piezoelectric microphone build on a micro-machined cantilever [Ref.12]. According to Lee's report, his cantilever model is much more compliant and can achieve more sensitivity compared to the other microphones, such as the clamped-clamped diaphragms. He also claimed that the sensitivity of the cantilever microphone has the highest of the ever-reported microphones with the micro-machined diaphragms. In addition, the relatively large deflections of the free end can produce significant acoustic output.

2.2 Design Model

The first step in building our model is to give its geometry. Since this device is aimed to implant into the human middle ear canal, and attached to the incus (or anvil, which is an anvil-shaped small bone or ossicle in the middle ear, that transmits sound vibration from the malleus to the stapes), the size of the whole structure is confined between the tympanic membrane and the incus. Therefore, the dimensions and the mass of the transducer are limited. As a consequence to this, the output of such a device is limited. The size of the transducer, which can be attached to the ossicle in the middle ear cavity, has a diameter of 3-4 mm and height of 2.4 mm. In that case, for our design, the size of the transducer must be smaller than the diameter of 2 mm and the height of 2 mm in order to be implantable in most human middle ear and we

can have enough space for future improvement by adding new components, such as feedback cancellation circuits or remote digital system.

The schematic cross section of our designed piezoelectric hearing aid is illustrated in Fig. 2. The transducer is composed of four layers of different materials. The supporting base is made of SiO_2. Above the base, a layer of PZT material is sandwiched by two layers of aluminum. The top surface of the structure is $1.8\times1.8\mu m^2$. This can nearly cover the whole incus, and can be attached with ease. With one end fixed in the ear canal, the sound pressure coming from the eardrum causes a vibration and consequently, the PZT-5H generates an electrical signal corresponding to the loading force. Meanwhile, the vibrating speaker hits the tympanic membrane and as a result, it generates a sound in the human ear. As we have mentioned before, this implantable hearing transducer can provide natural hearing sounds without any feedbacks.

Figure 2: Schematic cross section of piezoelectric hearing aid

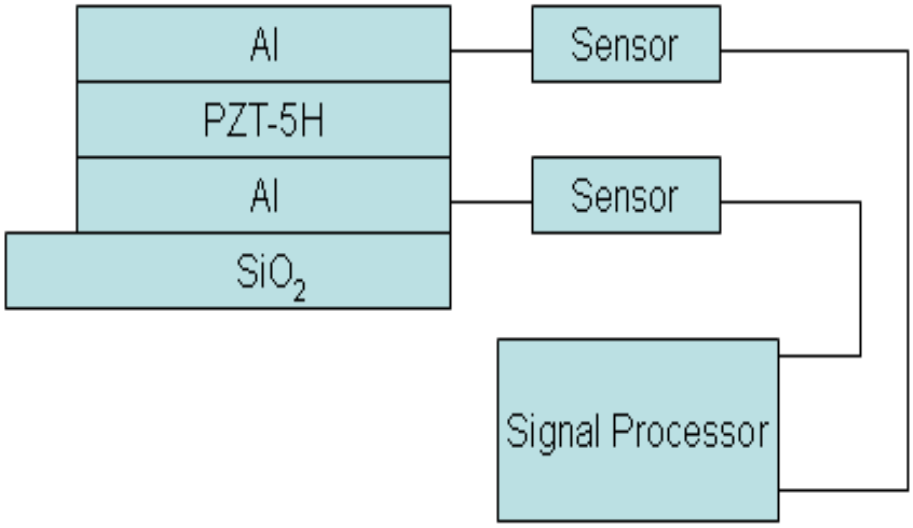

In our simulation work, first of all, the geometry of each component needs to be defined separately, and then joined together as a whole structure. The adjacent layers are firmly attached so the vibration, mechanical stress is generated between the adjacent layers since they have different Young's modulus coefficient. Secondly, the material properties of each component is given, including the Young's modulus, poison's ratio, density, piezoelectric coefficients, etc. After that, a detailed boundary condition is required. In our case, the vibrating transducer is firmly fixed at one end. In other words, the degrees of freedom on that end are set to be zero. Other parts of the device are free to move. A loading condition gives the external environment information, for example, the sound pressure applied on the transducer and the temperature at which the vibrating process is occurred. In order to obtain a precise result, a suitable mesh mode needs to be chosen. Different mesh mode may largely infect the precision of the result. Coarse mesh gives a rough data while extra fine mesh mode will bring a lot more unnecessary calculation, which takes more computation time. A more detailed discussion about mesh mode is included in Chapter 5. One important reminder is that an estimated value is essential before running the computation. This not only saves the calculation time but also gives a more accurate result.

2.3 Material Properties

In our design, we choose SiO_2 as our base material since SiO_2 provides a good abrasion resistance, electrical insulation and high thermal stability. It is insoluble in almost all kinds of acids, except hydrogen fluoride (HF). So it is a perfect material to apply MEMS techniques on this substrate.

Table 3: Material Properties of SiO_2

Young's Modulus (N/m^2)	7×10^{10}
Poisson's Ratio	0.17
Density (Kg/m^3)	2200
Thermal Conductivity ($W/m \cdot K$)	1.4
Relative permittivity	4.2
Thermal Expansion coefficient	0.5×10^{-6}
Heat Capacity ($J \cdot g^{-1} \cdot K^{-1}$)	0.73

For our conduction media, we use two layers of aluminum, since it has a good conductivity with extremely low cost. Also, aluminum can prevent the electrons from diffusing between the PZT and the silicon base.

Table 4: Material properties of Aluminum

Young's Modulus (N/m^2)	7×10^{9}
Poisson's Ratio	0.33
Density (Kg/m^3)	2700
Electrical conductivity	3.78×10^{7}
Relative permittivity	1
Thermal Expansion coefficient	2.3×10^{-5}
Heat Capacity ($J \cdot g^{-1} \cdot K^{-1}$)	0.9

PZT-5H is picked as our main piezoelectric material. According to Table.1, it is obvious that PZT-5H has high piezoelectric coefficient. In addition, it has a relatively low Young's modulus. This means that PZT-5H is best suit for hearing aids transducer since it requires the material to be flexible so it can achieve great vibration amplitude to generate a clear sound. More detailed piezoelectric parameters are listed in Table 5-10.

Table 5: Elasticity matrix of PZT-5H c^E (Pa)

1.3×10^{11}	8.0×10^{10}	8.5×10^{10}	0	0	0
8.0×10^{10}	1.3×10^{11}	8.5×10^{10}	0	0	0
8.5×10^{10}	8.5×10^{10}	1.2×10^{11}	0	0	0
0	0	0	2.3×10^{10}	0	0
0	0	0	0	2.3×10^{10}	0
0	0	0	0	0	2.3×10^{10}

Table 6: Coupling matrix, strain-charge form of PZT-5H d (C/N)

0	0	0	0	7.4×10^{-10}	0
0	0	0	7.4×10^{-10}	0	0
-2.7×10^{-10}	-2.7×10^{-10}	5.9×10^{-10}	0	0	0

Table 7: Coupling matrix, stress-charge form of PZT-5H e (C/m^2)

0	0	0	0	17.0	0
0	0	0	17.0	0	0
-6.6	-6.6	23.2	0	0	0

Table 8: Permittivity matrix, stress-charge form of PZT-5H ε^S

1704.4	0	0
0	1704.4	0
0	0	1433.61

Table 9: Permittivity matrix, strain-charge form of PZT-5H ε^T

3130	0	0
0	3130	0
0	0	3400

Table 10 : Compliance matrix of PZT-5H s^E (1/Pa)

1.7×10^{-11}	-4.8×10^{-12}	-8.5×10^{-12}	0	0	0
-4.8×10^{-12}	1.7×10^{-11}	-8.5×10^{-12}	0	0	0
-8.5×10^{-12}	-8.5×10^{-12}	2.7×10^{-11}	0	0	0
0	0	0	4.3×10^{-11}	0	0
0	0	0	0	4.3×10^{-11}	0
0	0	0	0	0	4.3×10^{-11}

2.4 Method

Piezoelectricity involves both the electrical and mechanical behavior of the material. To describe its electric field strength, the electric displacement D is usually written in the form

$$D = \varepsilon E \qquad \text{Equation 1}$$

where ε is the permittivity and E is electric field strength.

The Hooke's law describes the mechanical behavior:

$$S = sT \qquad \text{Equation 2}$$

where S is strain, s is compliance and T is stress.

The strain-charge form can be derived by combining the above two equations into so-called coupled equations:

$$\{S\} = [s^E]\{T\} + [d_t]\{E\} \qquad \text{Equation 3}$$

$$\{D\} = [d]\{T\} + [\varepsilon^T]\{E\} \qquad \text{Equation 4}$$

where d represents the piezoelectric constants, and the superscript E indicates a zero, or constant, electric field; the superscript T indicates a zero, or constant, stress field; and the subscript t stands for transposition of a matrix.

The strain-charge for a material of the crystal class (such as a poled piezoelectric ceramic, e.g. PZT) may also be written as:

$$\begin{bmatrix} S_1 \\ S_2 \\ S_3 \\ S_4 \\ S_5 \\ S_6 \end{bmatrix} = \begin{bmatrix} s_{11}^E & s_{12}^E & s_{13}^E & 0 & 0 & 0 \\ s_{12}^E & s_{11}^E & s_{13}^E & 0 & 0 & 0 \\ s_{13}^E & s_{13}^E & s_{33}^E & 0 & 0 & 0 \\ 0 & 0 & 0 & s_{44}^E & 0 & 0 \\ 0 & 0 & 0 & 0 & s_{44}^E & 0 \\ 0 & 0 & 0 & 0 & 0 & s_{66}^E = 2\left(s_{11}^E - s_{12}^E\right) \end{bmatrix} \begin{bmatrix} T_1 \\ T_2 \\ T_3 \\ T_4 \\ T_5 \\ T_6 \end{bmatrix} + \begin{bmatrix} 0 & 0 & d_{31} \\ 0 & 0 & d_{31} \\ 0 & 0 & d_{33} \\ 0 & d_{15} & 0 \\ d_{15} & 0 & 0 \\ 0 & 0 & 0 \end{bmatrix} \begin{bmatrix} E_1 \\ E_2 \\ E_3 \end{bmatrix}$$

Equation 5

$$\begin{bmatrix} D_1 \\ D_2 \\ D_3 \end{bmatrix} = \begin{bmatrix} 0 & 0 & 0 & 0 & d_{15} & 0 \\ 0 & 0 & 0 & d_{15} & 0 & 0 \\ d_{31} & d_{31} & d_{33} & 0 & 0 & 0 \end{bmatrix} \begin{bmatrix} T_1 \\ T_2 \\ T_3 \\ T_4 \\ T_5 \\ T_6 \end{bmatrix} + \begin{bmatrix} \epsilon_{11} & 0 & 0 \\ 0 & \epsilon_{11} & 0 \\ 0 & 0 & \epsilon_{33} \end{bmatrix} \begin{bmatrix} E_1 \\ E_2 \\ E_3 \end{bmatrix}$$

Equation 6

The piezoelectric sensing, which describes the electrical charge change from the piezoelectric cantilever after a force is applied across the face of the piezoelectric film can be written as:

$$V=ktT$$ Equation 7

where k is the piezoelectric voltage coefficient, and t is the thickness of the piezoelectric cantilever. T is the mechanical stress applied to the piezoelectric cantilever.

Since our transducer has a multimorph structure, the deflection of the cantilever is an important factor. This factor can be derived from the static equilibrium and strain compatibility between successive layers in the device, and can be written as:

$$Y = L^2\left(\frac{2d_{31}GA^{-1}C}{2 - GA^{-1}B}\right)$$ Equation 8

where L is the length of the cantilever beam, d_{31} is the piezoelectric coupling constant. A, B, C, and G are matrices that describe the parameters of the cantilever.

$$A = \begin{bmatrix} 1/A_1E_1 & -1/A_2E_2 & 0 & 0 \\ 0 & 1/A_2E_2 & 1/A_3E_3 & 0 \\ 0 & 0 & 1/A_3E_3 & 1/A_4E_4 \\ 1/A_4E_4 & 0 & 0 & 1/A_1E_1 \end{bmatrix}$$

Equation 9

where A_i, E_i are the area, the effective Young's modulus, of each component.

$$B = \begin{bmatrix} t_1 + t_2 \\ t_2 + t_3 \\ t_3 + t_4 \\ t_4 + t_1 \end{bmatrix}$$

Equation 10

$$C = \begin{bmatrix} E_2 - E_1 \\ E_3 - E_2 \\ E_4 - E_3 \\ E_1 - E_4 \end{bmatrix}$$

Equation 11

$$G = \frac{1}{\sum_{i=1}^{4} E_i I_i} \left[\left(\frac{t_1}{2} \right) \left(t_1 + \frac{t_2}{2} \right) (t_1 + t_2 + \frac{t_3}{2}) (t_1 + t_2 + t_3 + \frac{t_4}{2} \right]$$

Equation 12

where t_i, E_i, I_i, are the thickness, Young's modulus, moment inertia of the four layers.

However, the computation of such a process is quite complicated so we involved COMSOL® to help with the calculation. The technique behind this software is the finite element method (FEM), which is widely used in all kinds of computations for

engineering and physical problems. FEM is a numerical analysis technique to solve the differential equations. This method sub-divides a complicated domain into a series of smaller regions. The mechanical and electrical properties of these domains can be explored by solving the differential equations in each of the regions. In such a process, each region is regarded as an element and the process of subdividing a domain into a finite number of elements is referred to as discretization. All the elements are connected at specific points, which are known as nodes. The adjacent elements are assumed to be continuous along its common boundaries.

CHAPTER 3

THERMOELASTIC DAMPING FOR MEMS MIRRORS

The design of microstructures with a high quality factor (Q value) is of significant importance in many MEMS (microelectromechanical system) applications, including MEMS hearing aids. Thermoelastic damping can cause an intrinsic energy loss that affects the Q value of high-frequency resonance in those devices such as MEMS mirrors. This chapter deals with the simulation and analysis of thermoelastic damping of MEMS mirrors based on the finite element method. Four designs of MEMS mirrors with different geometric shapes are studied. In each model, the dynamic responses of the system subject to thermoelastic damping are compared to the computational results of undamped modes. This work is followed by a set of parametric studies on both the resonant frequency and Q value as functions of various representative parameters. These results are useful for early prediction of thermoelastic energy loss, not only in MEMS mirrors but also in more general MEMS resonators and filters.

3.1 MEMS mirrors

MEMS mirrors are widely used in modern high-tech industry, including high-speed Internet, wireless communication, biomedical system, robots, etc. For example, a MEMS mirror can be manufactured in the form of a tunable MEMS filter for dense wavelength-division-multiplexed (DWDM) optical networks [Ref. 13 and 14].

Techniques were developed to change the wavelength of a laser by tuning the cavity in the mirrors. However, the dynamic deflection of microstructures connected

to the mirrors under varying voltage can cause a structural resonance, which is associated with various damping mechanisms leading to energy dissipation. These mechanisms include i) viscous effects [Ref. 15]; ii) anchor losses [Ref. 16]; iii) squeeze film damping [Ref. 17]; and iv) the acoustic effects [Ref. 18]. However, it is strongly evident that thermoelastic damping, driven by the coupling between thermoelasticity and elastodynamics, is a dominant source of intrinsic damping in MEMS and NEMS resonators operating at high frequency [Ref. 19 and 20].

Briefly, thermoelastic damping occurs when a cyclic stress is applied to a material and the stress leads to an oscillatory deformation of the structure [Ref. 21]. The energy is lost irreversibly when the heat flows from the compressed part (hot region) to the stretched part (cold region) in the material. The lost energy can be evaluated by the measure of the quality factor, a factor that compares the time constant for decay of an oscillating system's amplitude to its oscillation period. Physically speaking, the Q value is 2π times the ratio of the toal energy stored divided by the energy lost in a single cycle. Equivalently, it compares the frequency at which a system oscillates to the rate at which is it dissipates its energy. A higher Q indicates a lower rate of energy dissipation relative to the oscillation frequency. While a lower Q indicates a large rate of energy loss and will lead to the reduction of the sensitivity and more power consumption.

The theory of thermoelastic damping was first established by Zener [Ref. 22], who developed a general theory for thin beams under bending. However, Zener's derivation involved some mathematical and physical simplifications. Lifshitz and Roukes [Ref. 23] successfully removed these simplifications, and derived an exact expression of the solution from the fundamental theories of thermoelasticity and elastodyanmics. The same technique was later extended to other problems involving

microplates of finite width [Ref. 24] as well as in-plane vibration of MEMS gyros [Ref. 25 and 26]. In addition, Sun et al. [Ref. 27] studied thermoelastic damping in beam resonators under a variety of boundary conditions using a special technique called “the finite sine Fourier transformation method”. Recently a research group also reported some results regarding the link between Zener's analytical solution for a simple reed in bending and the solutions of more complicated resonator shapes [Ref. 28 and 29]. Among all the numerical methods used to solve the problem of interest, the finite element discretization scheme has been proved the most successful one to date. For example, Silver and Peterson [Ref. 30] used a differential stiffness matrix to solve the thermoelastic damping problem for beams. Yi et al. [Ref. 31 and 32] developed a general eigenvalue scheme in conjunction with the finite element method to solve the problem in an arbitrary two or three-dimensional domain. (Although some earlier works already existed in the literature, e.g. Gorman [Ref. 33]). In fact, the finite element formulation for solving the thermoelastic damping problems has successfully been implemented in several widely used commercial packages including COMSOL® and ANSYS®. We will show the application of the COMSOL® software to solve the thermoelastic damping induced energy dissipation problem in MEMS mirrors for four different designs. Analytical approaches would otherwise be difficult to implement in the current problem due to the three-dimensional geometry and the complex boundary conditions involved. Parametric analyses are performed to investigate the effects of various design parameters on the resonant frequency and Q value [Ref. 34].

3.2 Methods

For a simply supported beam structure, analytical expressions were developed by

previous researchers to estimate the thermoelastic damping energy dissipation. According to Zener, the Q value can be calculated with a single thermal mode by:

$$\frac{1}{Q} = \left(\frac{E\alpha^2 T_0}{\rho C_p}\right)\left(\frac{\omega\tau}{1+(\omega\tau)^2}\right) \qquad \text{Equation 13}$$

where E is Young's modulus, α is the thermal expansion coefficient, T0 is the resonator's mean temperature at rest, ρ is the density, Cp is the heat capacity of the material, ω is the resonant frequency, and τ is the thermal relaxation time of the system. From this equation, it is not difficult to see that in order to obtain a high quality factor. The system must be designed in a way such that ω is as far from 1/τ as possible.

The natural frequency of an undamped, simply supported beam system can be calculated by:

$$\omega_0 = \frac{\pi^2 h}{L^2}\sqrt{\frac{E}{12\rho}} \qquad \text{Equation 14}$$

where L and h are the length and thickness of the beam, E is Young's modulus, and ρ is the density. The thermal relaxation time of a beam is given by:

$$\tau = \frac{\rho C_p h^2}{\pi^2 k} \qquad \text{Equation 15}$$

where k is the thermal conductivity. The above equations are only applicable to simply supported beam structure. For more complex structures and boundary conditions as involved in the MEMS mirror applications, a generalized eigenfrequency analysis is required to find the dynamic characteristics of the system. Particularly, the variables in the governing differential equations are expressed in a perturbation form with an exponential decay rate. Time is canceled in the resulting equations, leading to an eigenvalue equation. The eigenvalue λ of either a damped or

an undamped system contains the information about both the resonant frequency ω and the Q value. λ appears to be a complex value, and one can relate λ to ω and Q according to the following equations:

$$\omega_0 = \left| img(\lambda) \right| \qquad \text{Equation 16}$$

$$Q = \left| \frac{img(\lambda)}{2real(\lambda)} \right| \qquad \text{Equation 17}$$

where img(λ) and real(λ) are the imaginary part and real part of λ, respectively. In COMSOL®, the above eigenvalue scheme is integrated into the finite element formulation. The construction of the MEMS mirror computational model in COMSOL® followed a procedure as below: 1) the three-dimensional beam and mirror geometries were created individually and then merged together using the appropriate Boolean operations. The interior boundaries were then deleted. An external code was implemented to allow the changes of the geometric properties required in the parametric analyses. 2) The finite element mesh consisting of tetrahedron elements was generated using the built-in mesh generation functions. The local mesh density and element size were controllable through a set of meshing parameters. 3) The governing differential equation for heat conduction involving thermoelastic damping as follows was specified in the model description portion as required by the COMSOL® package.

$$k\nabla^2 T = \rho C_p \frac{\partial T}{\partial t} + \frac{E\alpha T_0}{(1-2\nu)} \frac{\partial(\varepsilon_x + \varepsilon_y + \varepsilon_z)}{\partial t} \qquad \text{Equation 18}$$

where εx, εy, εz are the strains in the x, y and z directions; ν is Poisson's ratio.

CHAPTER 4

FREQUENCY MEASUREMENT SYSTEM

During the past few years, many new technologies have been introduced to hearing aids for a better performance. For our future study of piezoelectric transducers [Ref.35], an accurate experimental study of its performance is needed. Vibration frequency is a major factor that affects the quality of a hearing aid. Among several existing measurement technologies, laser measurement is considered to be a precise approach for measuring the frequency properties for MEMS (micro-mechanical-electrical-system) devices. In this chapter, a piezoelectric transducer used as hearing aid speaker is demonstrated and an optical measurement method for frequency measurement of hearing aid transducer is discussed in detail. Our measurement system is based on Mach-Zehnder interferometer system. Experimental results show that the vibration of our sample can be accurately detected using a laser beam and spectrum analyzer. The vibration frequency is calculated by measuring the intensity variance. This system aims to provide a simultaneous optical measurement with high accuracy.

4.1 Introduction

There are many ways to measure the vibration frequency [Ref. 36]. The basic concept for frequency measurement is to obtain the unknown frequency from a reference frequency. Among all the various techniques available, laser measurement method is considered to be the best approach for high accuracy measurement. Laser interferometry is a fundamental concept used in laser measurement [Ref. 37]. Basically, it is a technique of using the pattern of interference. When two or more

laser light waves are traveling through the same medium, the superposition of these waves causes the interference. Compared to other light sources, laser light can operate with much longer beam paths, and the path differences are also greater than the other conventional interferometers, which is especially important for high precision measurement. Laser interferometry is widely used in all kinds of measurement for MEMS devices, including amplitude measurement, resonator frequency measurement, velocity measurement, etc.

Many researches have investigated the application of laser measurement. Currently, there are two types of interferometer that are generally used for frequency measurement. They are Mach-Zehnder interferometer [Ref. 38] and Michelson interferometer. Mach-Zehnder interferometer (MZI) system, which is named after physicists Ludwig Mach and Ludwig Zehnder, is commonly used in phase shift measurement. The phase shift is achieved by placing the testing sample in the path of one of two collimated laser light beams from a coherent light source. On the other hand, the Michelson interferometer is an interference pattern that is achieved by splitting a beam light into two separate parts, and by reflecting one of them, interference is produced when recombining them. However, compared to Michelson interferometer, Mach-Zehnder interferometer has more output ports, which makes the measurement system a lot easier to be adjusted. K P Zetie and S F Adams present a thorough investigation of Mach-Zehnder interferometer [Ref. 39]. Their work points out that reflection changes from high to low refractive index and those from low to high refractive index need to be well considered to obtain a precise measurement result. Also, Satoru and Takehiko [Ref. 40] have recently proposed an opto-ultrasonic sensor for piezoelectric resonator frequency measurement. According to their report, they measure the resonating frequency by detecting the refraction index deviation

based on piezoelectric vibration. Although their research work shows that the laser measurement requires a preciseness of set-up, still, it is regarded to be the best accurate measurement method. Other reports have shown that the laser measurement method can precisely measure very high vibration frequency, up to 1 MHz with only 10 KHz uncertainties [Ref. 41]. This unique character is especially important in the use of hearing aid applications [Ref. 42].

In our work, we developed an optical measurement system based on Mach-Zehnder interferometer. This system is aimed to detect the vibration frequency of an acoustic speaker. A spectrum analyzer is involved in order to read the wavelength and the intensity level of laser detected by the optical sensor. We are able to obtain an acceptable experimental result in a range with the vibration frequency up to 2 KHz. The entire system can be observed simultaneously and the accuracy of the entire system is also investigated.

4.2 Vibration frequency measurement module

Our measurement module is composed of three parts as shown in Figure 3, a laser light emitting source, several optical devices, including two lens, two mirrors and two beam splitters for transmitting laser light, and an optical sensor that is connected to a spectrum analyzer, which in our module is used as signal receiver. All the devices are firmly set on a stable surface, and the laser diode, mirrors and optical sensor are all set to be of the same height so the laser light emitted from the laser diode can reach into the optical sensor. For our laser light source, we are using a He-Ne laser. It provides a visible red light that has a wavelength of 632.8nm. Here, we considered the speed of laser light in air is the same speed of light c in vacuum. When the laser light is emitted from the laser source, it is collimated in order to obtain

a parallel light beam. This is achieved by placing a positive lens to converge the spread laser light from the light source. The converged light beam passes through the first beam-splitter and is divided into two separate parts. One of the laser beams propagates straight through the beam-splitter and is referred to as “laser 1”, while the other laser beam, “laser 2”, is refracted in 90 degree by the beam-splitter and travels perpendicular to laser 1. This means that laser 2 has a phase change of one-half a wavelength since the reflection or refraction at the surface of a beam-splitter with a lower refractive index will cause a phase shift, meanwhile laser 1 has a constant phase change since the speed of light is slower when it is passing through the beam-splitter that has a greater refraction index of vacuum, and this will cause a phase shift proportional to the distance of the laser traveled in the beam-splitter. After laser 2 is refracted by the beam-splitter, a mirror reflects it. The mirror is placed 45 degree to the emitting laser light, so the reflected laser 2 is now parallel to laser 1. This also gives a phase change of one-half a wavelength to laser 2. This is because the medium behind the mirror (glass) has a higher refractive index than the medium the light is traveling in (air). Laser 1 goes directly through the second beam-splitter and reaches the optical sensor that is connected to the spectrum analyzer with an optical fiber. Laser 2 that is reflected by the first mirror will be reflected again by another mirror placed right next to the second beam-splitter. So laser 2 will be reflected again by 90 degree, which means there is another one-half a wavelength phase change. And the reflected laser 2 will go into the second beam-splitter. After the refraction in the second beam-splitter, which brings a one-half wavelength phase change for laser 2, both of the laser lights are incident on the second beam-splitter and interfere with each other. Adding up all these phase changes, we see that the total difference between the two paths is that laser 1 has gone through all the optical devices with a constant phase

change proportional to the distance that laser traveled in the beams-splitter, while laser 2 has a total phase change of one-half a wavelength after all the refraction in the beam splitter and reflection from the mirrors. Therefore, there will be a complete destructive interference when these two lasers are recombined at the second beam-splitter. An optical sensor then detects the phase interference. All the information is then transmitted to a spectrum analyzer. The wavelength and the intensity level are illustrated on the spectrum, and the data are recorded. However, there are several assumptions we made in this whole system, one is that any absorption of the laser power caused by the beam-splitter or mirrors is neglected, and the environmental factors including temperature and humidity are neglected for simplicity.

In our measurement system, we placed our testing sample, which is an acoustic speaker, in the way where laser 1 propagates, right between the two beam-splitters. A solid beam is attached to the surface of the speaker's membrane. Therefore, when the speaker is vibrating under an input electrical signal, the membrane forces the beam to vibrate at the same frequency as the speaker. Then the vibrating beam blocks the way that lasers 1 travels repeatedly. This will result in an intensity level change in the optical sensor that is detected by the optical sensor and the spectrum analyzer reads the data simultaneously.

Figure 3: Diagram of optical frequency measurement system

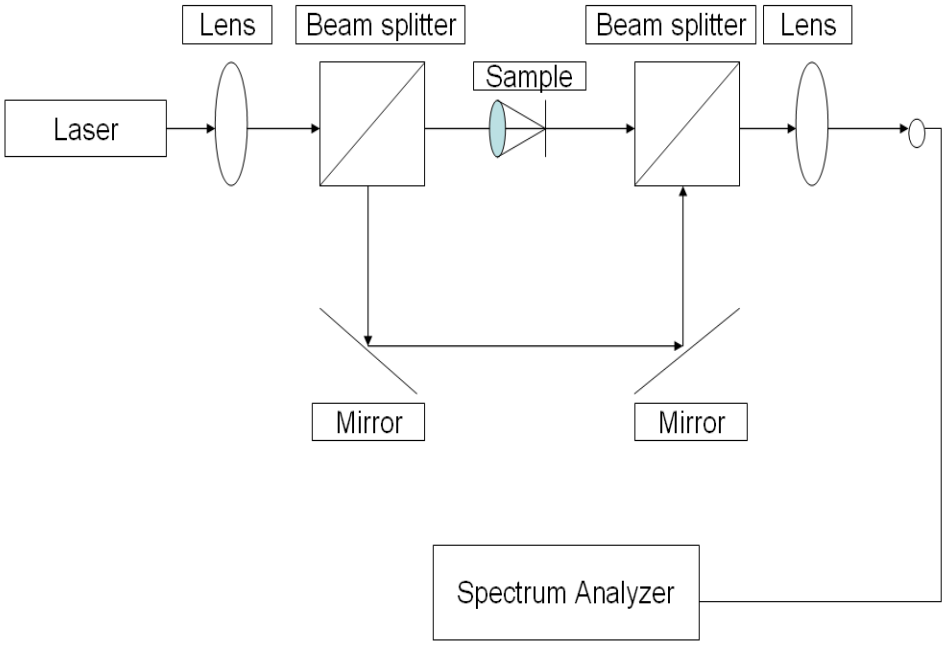

4. 3 Principles of Optical detection

In our vibration frequency measurement system, a continuous light is divided into two paths. One light propagates through the vibration speaker side, and the other light propagates through the optical phase shifting side with two mirrors. The two light beams are recombined using a beam-splitter and detected by an optical sensor connected to a spectrum analyzer.

The electric fields of the light beam passing straight through the two splitters can be expressed as

$$E_1 = A\exp(j\omega t) \qquad \text{Equation 19}$$

where ω is the angular frequency of the light beam.

For the other light beam that travels in the different path can be expressed as

$$E_2 = B\exp[j(\omega t + \theta + \phi)] \qquad \text{Equation 20}$$

where θ is the phase shift due to the optical length difference between the two paths, and ϕ is the phase shift caused by the vibration of the speaker. Phase shift ϕ is expressed by

$$\phi = \phi_0 \cos \Omega t \,, \qquad \text{Equation 21}$$

where Ω is the angular frequency of the piezoelectric vibration.

The detected signal is

$$I = K(E_1 + E_2)(E_1 + E_2)^*$$

$$= K(A^2 + B^2) + 2KAB\cos(\theta + \phi)\,. \qquad \text{Equation 22}$$

As we can see from (4), the first term indicates the DC component and the second term shows the modulated AC component due to the vibration of the speaker.

It is obvious that the signal component I depends on the optical path difference θ.

Let us assume a case where $\theta = \pi/2$, and K=1 for simplicity, therefore, I can be written as

$$I = V + 2AB\sin\phi = V + 2AB\sin(\phi_0 \cos \Omega t). \qquad \text{Equation 23}$$

where V represents the constant DC value. The sinusoidal part of Equation. 17 can be expanded by using the theory of Taylor series, and we can find out that the amount of phase shift caused by the vibration of the speaker is very small so only the first term of the Taylor series is significant, and therefore, we can simplify Equation. 17 as:

$$I = V + 2AB\phi_0 \cos \Omega t. \qquad \text{Equation 24}$$

Equation 6 also indicates that the signal amplitude is proportional to the phase shift amplitude ϕ. This is mainly because the phase shift amplitude ϕ is proportional to the vibration amplitude.

CHAPTER 5

RESULTS AND CONCLUSION

This work is the first step toward a final research of MEMS piezoelectric hearing aid. As an initial study, the basic structure of a PZT-5H based piezoelectric transducer is determined and the physical performance of such a device was investigated. Further, we looked into the thermal effect of the transducer and we extend our work to the thermoelastic damping in MEMS mirrors. For the sack of our future work, we also developed a frequency measurement system using optical devices.

5.1 Results

A. Piezoelectric transducer

An implantable middle ear MEMS piezoelectric transducer is designed for patients who suffer from a lacking of sufficient resiliency to transmit mechanical vibrations between the tympanic membrane and the oval window.

First, we fully investigate the basic performance of a piece of PZT-5H cantilever. A simulation of the PZT-5H is analyzed with different thickness to examine the physical vibration properties of the cantilever. Due to the confined space in the middle ear, the top surface of the cantilever is limited at 1.8×1.8 mm^2, this surface area can exactly cover the whole incus. We then try different thickness of the PZT-5H from 0.4 μm to 1.2 μm to see the vibration deflection difference at the tip of the cantilever. In this simulation, we applied a sound pressure of 20Pa on the top surface of the cantilever. The applied pressure induce the cantilever to vibrate, and generates a voltage difference from the top and bottom. From the result data presented in Table 11, we can conclude that with a certain surface area, the cantilever has a small deflection

at the tip when the thickness of the cantilever is large rather than small. Mechanically speaking, this can be simply explained as increasing the thickness of the cantilever beam will bring down the flexibility of the structure. However, with three other components in our MEMS piezoelectric transducer, this conclusion may not hold since composite material is not so straight forward and has a much more complex situation compared to single layer materials.

Table 11: Deformation at the tip of a PZT-5H cantilever beam responds to an increasing thickness with a fixed surface $1.8\times1.8mm^2$

Thickness (μm)	0.4	0.6	0.8	1	1.2
Deformation at the tip (μm)	88.75	13.04	5.99	3.00	1.75

For our final design, we use SiO_2 as our base substrate. Above the base, we have the PZT-5H material sandwiched between two layers of aluminum. The whole device is fixed at one end on the incus as a cantilever beam. We applied various thicknesses for the piezoelectric material to see the geometry effect on the vibration performance. The simulation work is done in COMSOL. The surface of the device is meshed in 324 elements, each elements is a $0.1\times0.1mm^2$ square. The mesh elements we are using on the thickness are 0.1mm. The results are listed in Figure 4.

Figure 4: Deflection of a piezoelectric cantilever

Vs. Thickness of the cantilever

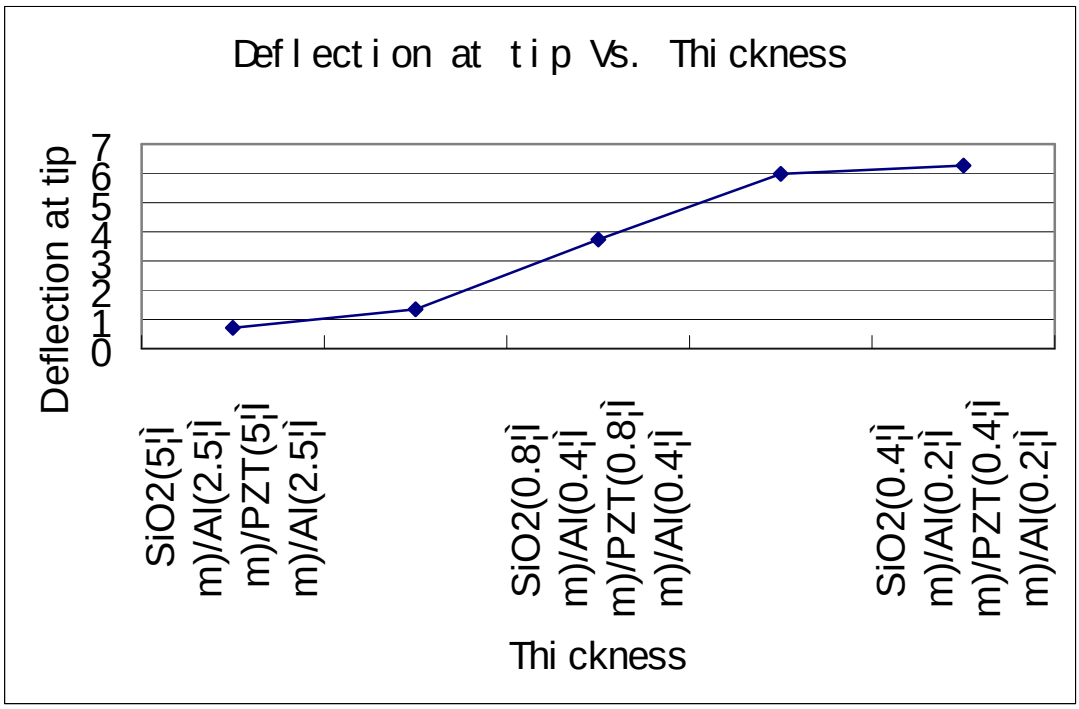

We can conclude from Figure 4 that over the thickness of 10μm barely gives any deflection at the tip of the cantilever. In other words, such a sound pressure is not enough to generate vibration to the cantilever. As a consequence, few electrons can be produced. We can also find that the cantilever, which has a total thickness of 1.8μm has a comparable large deflection of 6 μm. It has a SiO_2 substrate of 0.6μm, two Aluminum layers, each has a thickness of 0.3μm, and PZT-5H layer of 0.6μm thick, Smaller thickness than that does provide larger deflection, but considering the fabrication complexity that brings, it is unnecessary for going smaller thickness than 1.8μm. This size can be perfectly fits into any human's ear canal, and there is plenty of room for other components to be added onto the device for future improvement.

Figure 5: Deformation shape of a 1800×1800×1.8μm^3 PZT-5H based transducer under the sound pressure of 2×10^{-2} Pa

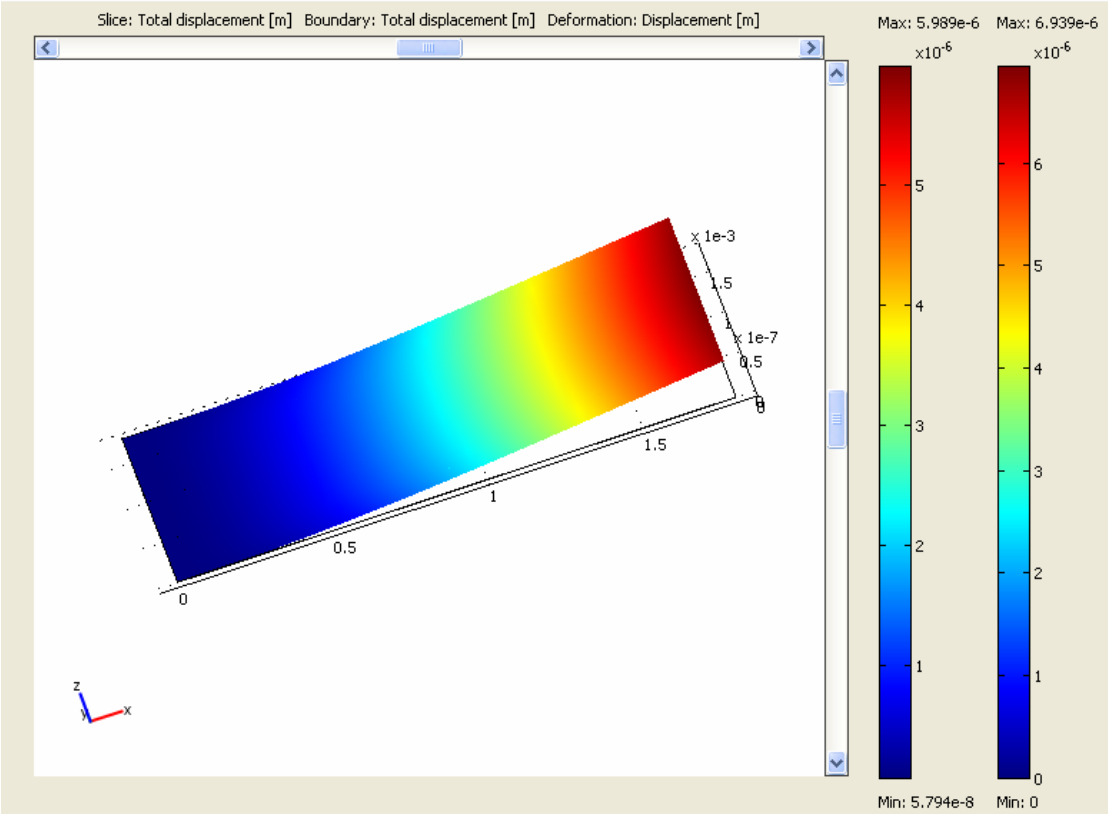

B. Convergence Tests of thermoelastic damping

We first performed a parametric analysis on the effect of the element number on the accuracy of the beam results. The commercial finite element code Abaqus CAE® was used. A simply supported beam was divided into a number of elements in the longitudinal direction and the natural frequency of resonance was computed using a generalized eigenfrequency analysis.

The beam size used was 0.1μm×0.1μm×1μm. The computational result is shown in Fig. 6. Apparently it is seen that the resonant frequency becomes asymptotic when the element number increases. In comparison to the theoretical solution of the undamped resonant frequency, the finite element results are sufficiently accurate when the element number is greater than around ten. However, an element number less than five could result in an appreciable inaccuracy in the solution. In practice, ten elements along the length should be considered as the minimum requirement for the beam problem under investigation. On the other hand, too many elements will make the computation cumbersome and should be avoided.

Figure 6: Convergence test showing the relationship between the resonant frequency and the finite element number for the first undamped modes of a simply supported beam.

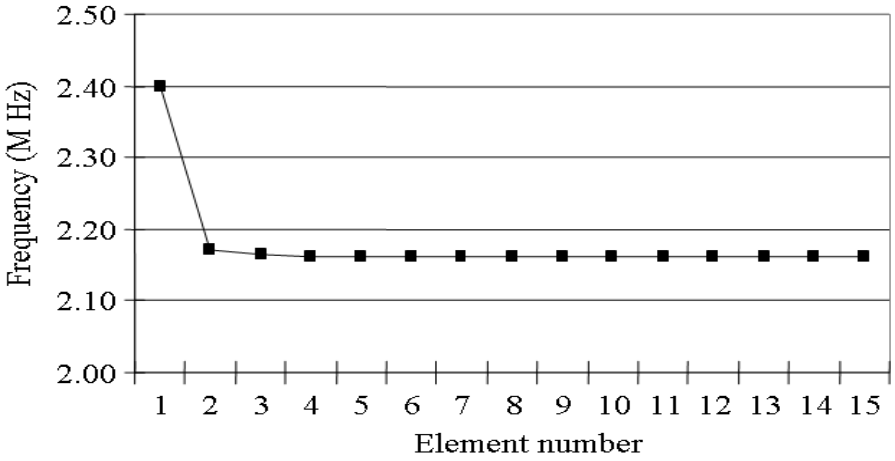

Four distinct MEMS mirror designs are shown in Fig. 7 were then analyzed and compared to each other. The material used for both the mirrors and the beams are polysilicon, which has widely been used in the manufacturing of surface-micromachined devices. For each of the four designs, multiple resonant modes could be excited and the different modes correspond to different resonant frequencies as well as Q values (as shown in Table 10). Not all of the modes, however, are important in engineering practice (e.g, some higher order modes are difficult to excite in real applications). In the current study, we focus on the first dominant mode (namely, the mode of the lowest resonant frequency) only. The information for higher order modes can be inferred from the results of the first mode.

Figure 7: Four different MEMS mirror models

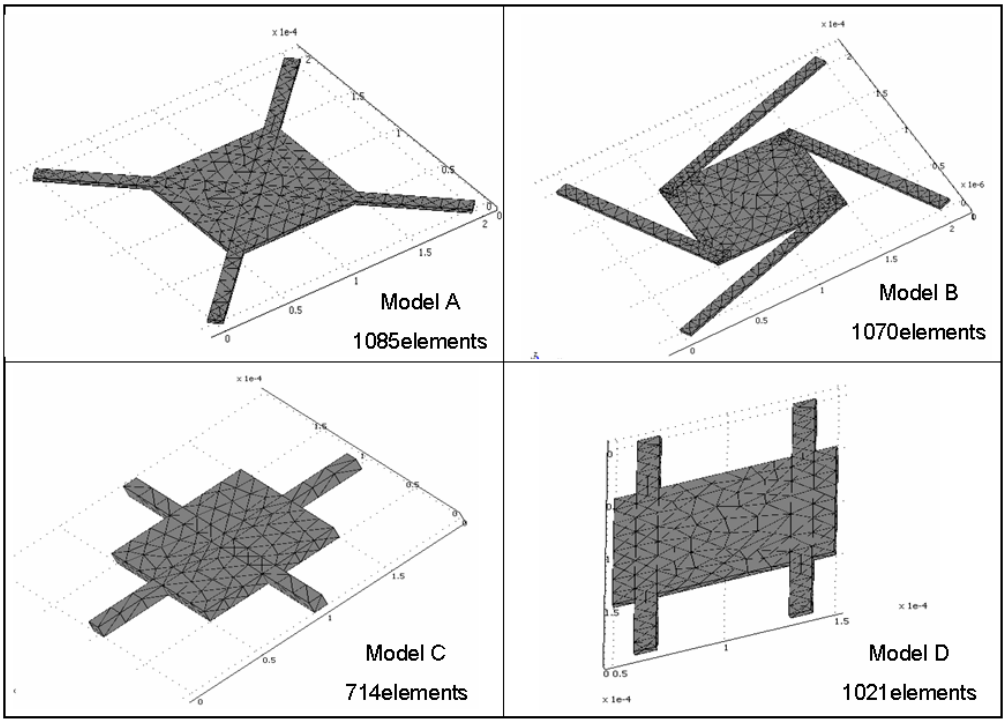

In all the four models, the peripheral beams connected to the central mirror are assumed fixed at the end; the mirror in the middle is free to vibrate. Both the beams and the mirror have the same thickness. The entire device is considered to be thermally insulated and the initial temperature is set to 300K.

In this part of the study, we first investigated the effect of the mirror size on the resonant frequency. From the results shown in Fig. 8(a) we found that the resonant frequencies in the presence of thermoelastic damping for all the models were close to the frequencies of the undamped modes. The results also show that the frequency drops when the mirror size increases. This is because the device can be approximated as an equivalent spring-mass system in which the mass increases with the mirror size. Although the equivalent spring constant also changes with the mirror size at the same time, the effect of the mass will dominate, leading to a lower resonant frequency.

In addition to the mirror size, there are several other geometric factors that were taken into consideration. One of these is the beam width. In the present study, we used model A to investigate the relationship between the beam width and the eigenfrequency of the model. The result in Fig. 9(a) shows that the eigenfrequency increases with the beam width. This can be explained again by considering the entire device as an equivalent spring-mass system. An increase of the beam width will increase the equivalent spring constant, and therefore raise the resonant frequency. In view of this, the MEMS mirror should be designed in a way such that the beams' width is sufficiently large to avoid any possible structural resonance with external vibrations.

Model B is a design with four beams connected to the corners of the central mirror at an inclined angle. The results in Fig. 10(a) show that the frequency decreases with the mirror size. We also investigated the frequency as a function of the

included angle between the beam and the mirror. Figure 11(a) shows that the frequency decreases with the angle. It can be explained as follows: when the angle increases, the distance between the equivalent mass center and the fixed point of the beam increases and makes the spring system more flexible. This will result in a reduced spring constant and therefore the resonant frequency is raised. We next investigated model C. Again, the resonant frequency decreases with the mirror size, as shown in Fig. 12(a). The impact of the beam thickness is shown in Fig. 13(a), from which we can see that the frequency changes with the beam thickness nearly along a straight line. This is consistent with the fundamental beam theory, in which the predicted frequency is linearly dependent on the beam thickness. In model D, there is nothing unusual for the relationship between the frequency and the mirror size (Fig. 14(a)). However, Fig. 15(a) shows that the resonant frequency increases with the beam spacing, although this change is much smaller than the changes caused by other factors. (In fact, for both damped and undamped models, the maximum change in the resonant frequency is less than 5%.)

Figure 8: Frequency (a) and quality factor (b) as functions of the mirror size in model A.

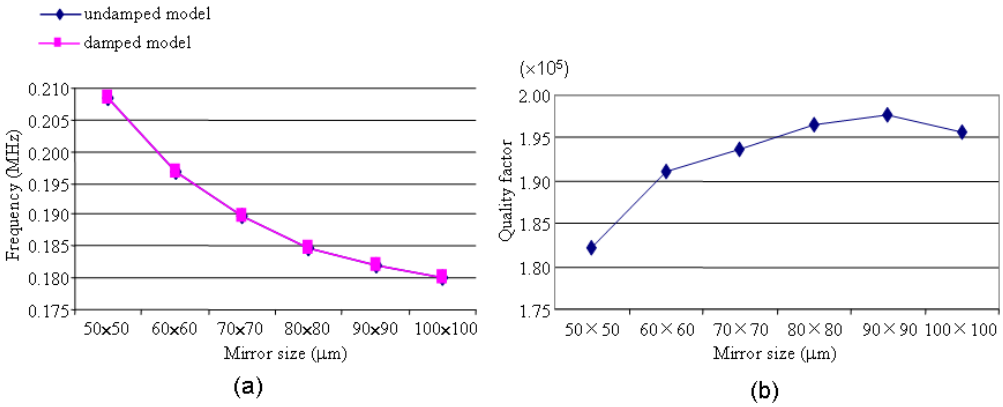

Figure 9: Frequency (a) and quality factor (b) as functions of the beam width in model A.

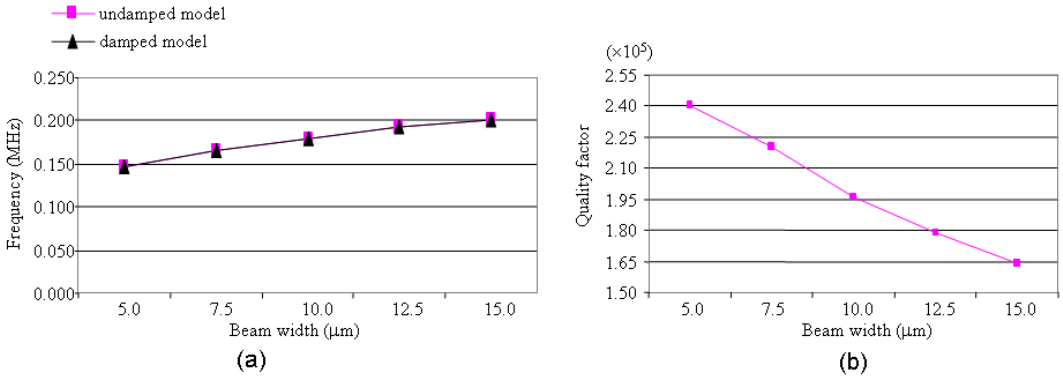

Figure 10: Frequency (a) and quality factor (b) as functions of the mirror size in model B.

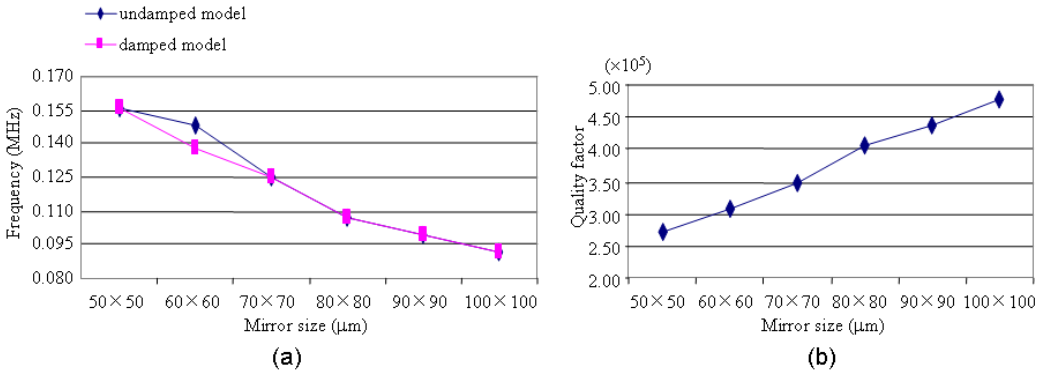

Figure 11: Frequency (a) and quality factor (b) as functions of the angle between two adjacent beams in model B.

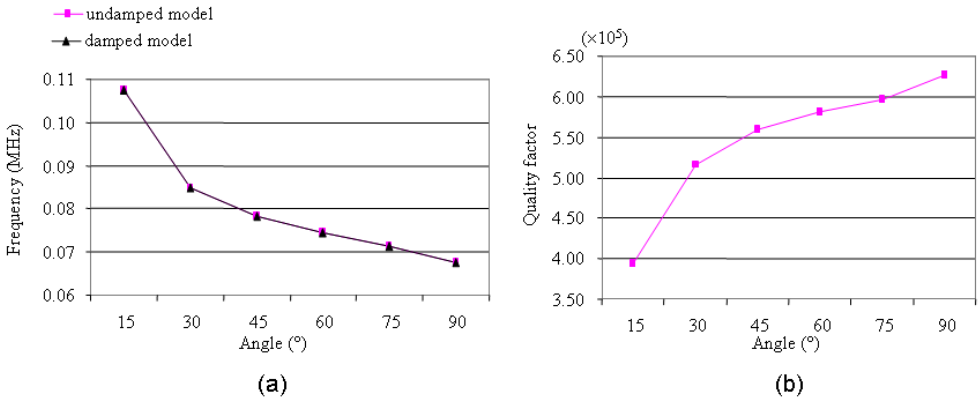

Figure 12: Frequency (a) and quality factor (b) as functions of the mirror size in model C.

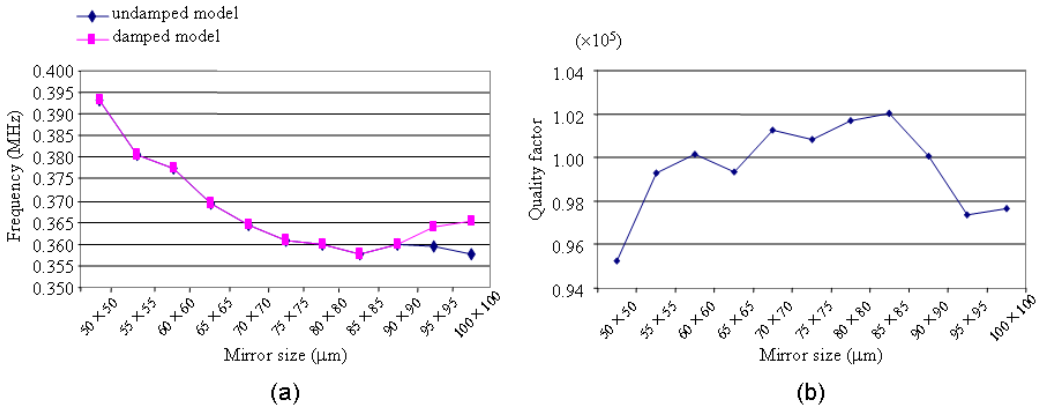

Figure 13: Frequency (a) and quality factor (b) as functions of the beam thickness in model C.

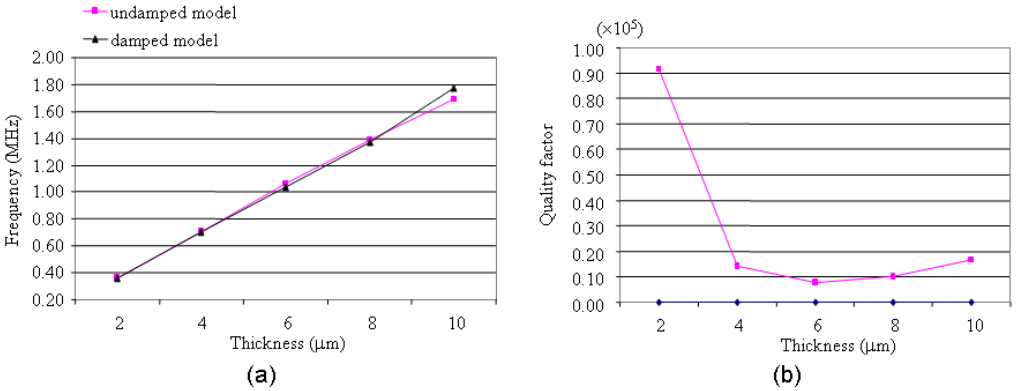

Figure 14: Frequency (a) and quality factor (b) as functions of the mirror size in model D.

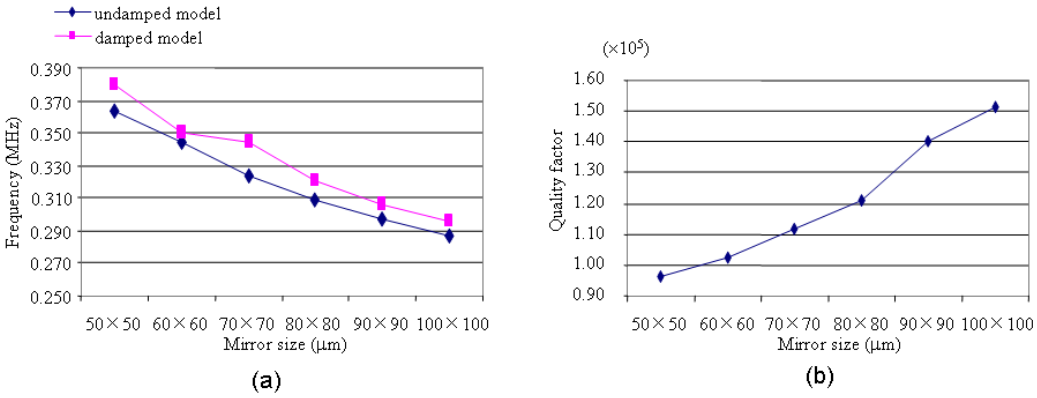

Figure 15: Frequency (a) and quality factor (b) as functions of the beam spacing in model D.

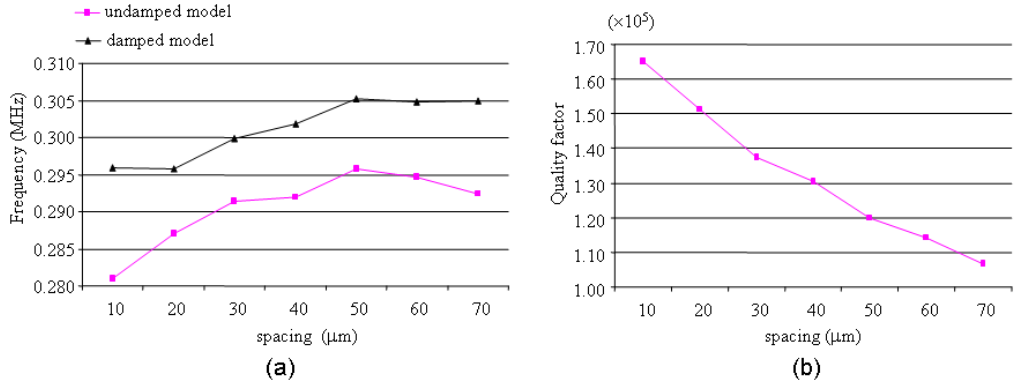

Quality factor is a major measurement to the energy dissipation. In fact, the magnitude of the energy loss largely relies on two factors, which are the resonant frequency and the structure's thermal relaxation time constant. The thermal relaxation time constant is the effective time that the material requires to relax after an applied constant stress or strain. Therefore, the effect of thermoelastic dissipation, which consequently leads to the damping, is most pronounced when the vibration frequency is close to the thermal relaxation frequency. The impact of geometric changes on the Q value has been studied for all four models.

In our study, we applied different mirror sizes in each model to compute the quality factor. Among all the mirror sizes being investigated for Model A (Fig. 8(b)), it has been found that the 90μm×90μm×2μm mirror size has the largest quality factor (1.98×105) among all the variable geometries. This means that this mirror size has the least energy loss induced by thermoelastic damping. Comparing the quality factor to the resonant frequency reveals that there is not a monotonic relationship between the quality factor and the frequency. In fact, when the real part of the eigenfrequency decreases, the imaginary part of the eigenfrequency could decrease more rapidly than the real part, which leads to an increase of the quality factor. The quality factors of model B and D increase with the mirror size as shown in Figs. 10(b) and 14(b). By comparing the quality factor of model B with other models of the same parameters, it is easy to find that model B has the largest quality factor. In fact, Model B with a mirror size of 100μm×100μm×2μm has the higher Q value (~4.8×105) among all the four designs A through D. For model C, the quality factor does not exhibit linear changes (Fig. 12(b)). Among all the results obtained for Model C, the quality factor corresponding to the mirror size 85μm×85μm×2μm is the greatest. However, this value is much smaller than model A or model B.

In Model A, the Q value was obtained by varying the beam width. According to the results, it has been found that the mirror with a wide beam has a much smaller Q value than the one with a narrow beam (as shown in Fig. 9(b)). This is consistent with the results reported in the literature showing that the quality factor decreases with the elastic modulus. In model B, the included angle between the beam and the mirror was varied in the analysis and the significant changes in the quality factor can be seen in Fig. 11(b). The Q value reaches the highest point when the angle is 90 degree. In Model C, the effect of the beam thickness was investigated. The quality factor has a relatively large value when the device is thin, and the value decreases rapidly when the thickness is increased (as shown in Fig. 13(b)). On the other hand, in Model D the quality factor decreases when the spacing between two adjacent beams is increased (as shown in Fig. 15(b)). Again these results can be explained by approximating the device as an equivalent single beam system and they are consistent with both the analytical and numerical results reported in the literature.

C. Frequency measurement results

Our measurement method is based on the experimental data read from the spectrum analyzer. Basically, the optical sensor detects the two laser lights coming out from the second beam splitter. The interference of these two lasers causes an intensity level change that is detected by the optical sensor. Then, all the information, including the wavelength, the intensity, is transmitted to the spectrum analyzer with an optical fiber. The optical waveform is shown on the spectrum analyzer.

We first examined our measurement system without any testing sample (Fig.16). As we can see from the spectrum, the central wavelength that we detected from the spectrum analyzer is at 1265.78nm. This is almost twice the wavelength of our laser

light source, which means that the central frequency shown on the spectrum in the second harmonic wavelength of the laser. This is a nonlinear optical process in the spectrum analyzer. The photons detected from the optical sensor are combined with a nonlinear material, and form new photos with twice the energy. This means the newly formed photon has doubles the frequency and half the wavelength of the initial photons. This method provides an easier detection of the second harmonic wavelength and doubling the frequency makes the laser more efficient. In this spectrum, the reference level is set to be -73.01dBm, and the sensitivity is -85.03dBm. The span of the spectrum is 20Hz, from 1255.781nm to 1275.781nm, as we can see, without any testing sample in the system, the intensity level detected is -77.563dBm. This gives the power level of the laser source since we assume there is no absorption in the optical devices.

Using the same method, we tested a set of different input signals and checked our experimental result with the result from a beam chopper. Table 3 illustrates both the experimental result and the theoretical result of the intensity level with different vibration frequency. Due to the limitation of our optical device, our measurement the highest frequency we can accurately measure is up to 2 kHz. However, we find that our system can provide a relatively accurate measurement with 7.7% error at most. The error is mainly caused by the absorption of the optical device, which makes the experimental result a little bit smaller than the theoretical result. During the measurement, we locked the reference intensity level to be -73.01dBm, and the sensitivity is set to -85.03dBm. All the observing spectrums are set to have a span of 20Hz, from approximately 1255nm to 1275nm, since the central frequency is estimated to be 1265.6nm, which is the second harmonic wavelength of the laser source.

Figure 16: Spectrum of optical frequency measurement system with no testing sample

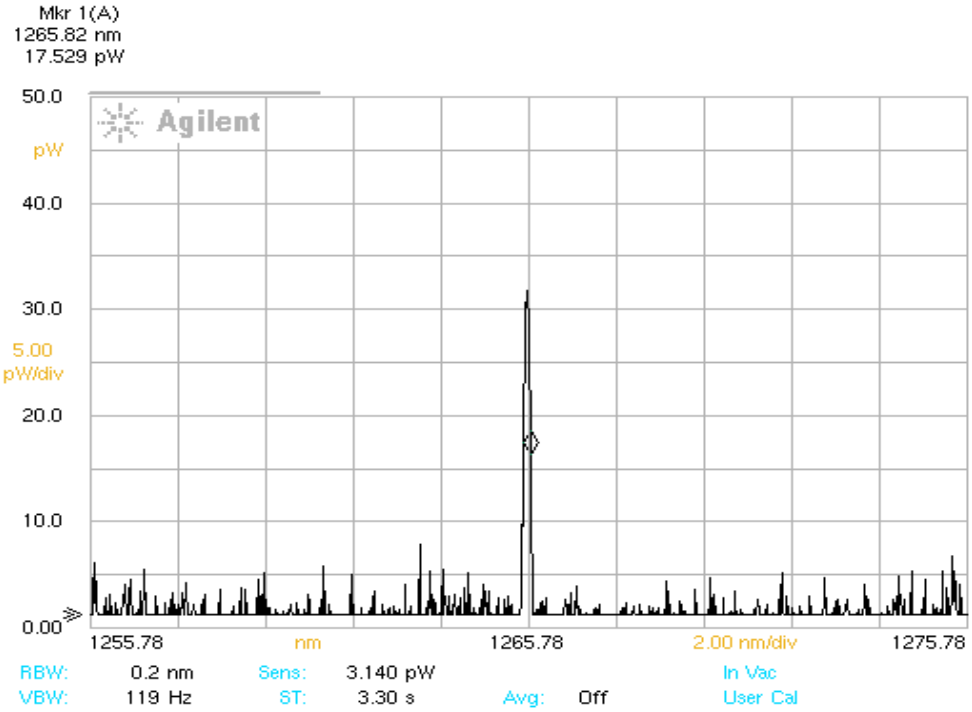

Table 12: Theoretical and experimental result of intensity level vs. vibration frequency

Vibration Frequency (Hz)	0	200	400	600	800	1000	1200	1500	1800	2000
Intensity (Experimental)	-77.6	-79.8	-79.8	-79.5	-69.1	-69.8	-69.8	-69.3	-70.1	-70.5
Intensity (Theoretical)	-77.6	-77.6	-77.6	-77.6	-65.1	-65.1	-65.1	-67.1	-65.1	-65.1

We also examined the wavelength detected by the optical sensor (Fig. 17). As we expected, the wavelength is approximately twice the value of the laser source. This has been explained as the second harmonic wavelength caused by the spectrum. It is obvious to find that the wavelength is 1265.821nm in the range from 0 Hz to 500 Hz, and the wavelength changes to 1265.841nm when the frequency reaches 600 Hz and higher. This can be caused by many reasons. For example, one of the reasons might be unstable connection between the attached beam and the membrane. The beam vibrates with its own resonant frequency may influence the whole vibrating system. Other factors that cause this problem may include environmental influence, such as temperature, and even the reflection from the optical sensor may have a huge impact on the accuracy of our measuring system. However, by studying the error of the variance, we find that the error of the result is within 0.001%, so these negative factors can be completely neglected.

Figure 17: Wavelength over vibration Frequency

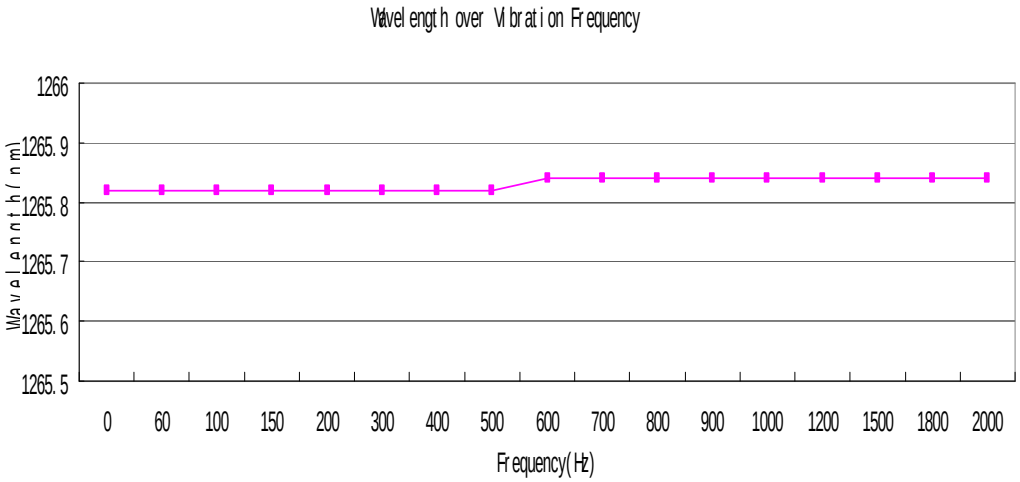

5.2 Conclusions

A set of parametric analyses has been performed to investigate physical vibration of a MEMS piezoelectric transducer. The PZT-5H material properties are studied and the material components of our final design are well chosen. From the simulation result, we can conclude that increasing the size of the device will leads to a smaller deformation at the tip of the cantilever. Physically speaking, enlarge the size leads to an increasing hardness of the structure, and it makes the device hard to bend. As we have mentioned before, transducers for different purposes requires different hardness or softness. Since this transducer is applied in hearing aids, it requires the cantilever to generate a large deflection at the tip so it can hit the ear ossicle hard. Our final model is well designed based on the size of the human's ear canal. We tested the transducer with a sound energy and observe its deflection response to the loading condition. The simulation result is obtained by using finite element method and as we can see that this transducer produced a relatively large deflection, which means that it can be applied to hearing aid applications.

The energy dissipation induced by thermoelastic damping in MEMS mirrors is fully investigated. The impact of different design schemes was studied. Because of the geometric complexity of the MEMS mirrors, the finite element method was applied. Based on the numerical results obtained from the four distinct designs, it has been found that the resonant frequencies of the damped and undamped modes are generally very close. An increase of the central mirror size will lead to a decrease of resonant frequency whereas the quality factor typically increases. On the other hand, an increase of the thickness of the entire structure will lead to a higher resonant frequency yet a lower quality factor. The beam section also plays an essential role: increasing the beam width leads to higher frequency, but a lower quality factor.

From the standpoint of minimizing energy loss due to thermoelastic damping, Model B with a mirror size of 100μm×100μm×2μm and an included angle of 90° between the peripheral beam and the central mirror exhibits the highest Q value and is therefore the best design among the four models being investigated. However, in practice various factors may be considered simultaneously: for example, the optimization of the configuration with the greatest deflection range might have a higher priority than the consideration of energy consumption.

The techniques used in this work can be readily extended to solve thermoelastic damping problems involved in more complex geometries. However, the computational time increases considerably with the degrees of freedom, especially when the damping is coupled with other physical processes such as electrostatic deformation. Development of reduced-order models, which is part of our future work, is therefore essential to enhance the numerical efficiency in the computation.

Furthermore, we described an optical system for vibration frequency measurement with high accuracy. The frequency measurement system is based on Mach-Zehnder interferometer system, and it is used to test acoustic speaker with a vibration frequency up to 2 kHz. Although the wavelength spectrum is shown in the second harmonic wavelength of our laser source, the intensity level can be easily detected simultaneously.

We examined our system by using a beam chopper and a comparison of the result from the testing speaker and a beam chopper is discussed by its accuracy. Our experimental result indicates that the spectrum intensity decreases with an increasing vibration frequency of the speaker. Still, there are a few things to improve to optimize our system. Further improvement will be focusing on improving the accuracy of the experimental result by eliminating some negative environmental factors, and reduce

the absorption of the signal power from optical devices. However, this highly sensitive optical measurement system can still offer a high accurate measurement result and it is expected to help develop new hearing aid device.

LIST OF REFERENCE

[1] Jack W Judy, “Microelectromechanical systems (MEMS): fabrication, design and applications”, Smart mater. Struct. 10 (2001) 1115-1134.

[2] Babu Lal Gupta, “MEMS Microphones: A Global Technology, Industry and Market Analysis”, Electronics. Ca publications. #IR-ET105, July 2007.

[3] Eung-Pyo Hong, Min-Kyu Kim, Ii-Yong Park, Seung-ha Lee, Yongrae Roh, and Jin-Ho Cho, “Vibration Modeling and Design of Piezoelectric Floating Mass Transducer for Implantable Middle Ear Hearing Devices”, IEICE Trans, Fundamentals, Vol. E90-A, NO. 8 August 2007.

[4] Q. C. Xu, S. Yoshikawa, J. R. Belsick, and R. E. Newnham, “Piezoelectric Composites with High Sensitivity and High Capacitance for Use at High Pressure”, IEEE on Ultrasonics, Ferroelectrics, and Frequency Control, Vol. 38. No. 6. November 1991.

[5]Harry Goldstein, “ The Irresistible Transistor”, IEEE, October 7, 2008.

[6] Wen H. Ko, J. Guo, Xuesong Ye, R. Zhang, D. J. Young, “MEMS Acoustic Sensors for Totally Implantable Hearing Aid Systems”, IEEE.

[7] Ren Tian-Ling, Zhang Lin-Tao, Liu Li-Tian, and Li Zhi-Jian, "Design Optimization of Beam- Like Ferroelectrics-silicon Microphone and Microspeaker," IEEE Transactions on Ultrasonics, Ferroelectrics, and Frequency Control, Vol. 49, No.2, Februtary 2002 5.

[8] Sherif A. Saleh, Hamed Elsimary, Amal Z. Mohamed, Hesham F. Hamed, “Design of Piezoelectric cantilever microphone and Its MEMS acoustical Circuit for Hearing Aid Devices”

[9] “Piezoceramic Materials”, www.piceramic.de

[10] Julian W. Gardner, Osama. O. Awadelkarimn, "Piezoelectric Cantilever Microphone and Microspeaker, "Journal of Microelectromechanical Systems, Vol. 5, No. 4, December 1996.

[11] Mathew C. Celina, Tim R. Dargaville, Pavel M. Chaplya, Roger L. Clogh, "Piezoelectric PVDF Materials Performance and Operation Limits in Space Environments", MRS.

[12] Seung S Lee. Robert P. Ried, and Richard M. White, "Piezoelectric Cantilever Microphone and microspeaker", Journal of Microelectromechanical System, Vol. 5, No. 4, December 1996.

[13] Y. Guan and M. A. Matin, "Design and analysis of MEM-micromirrors for vertical cavity surface emitting lasers," *Microwave and Optical Technology Letters* **37,** 410-413 (2003).

[14] Y. Guan and M. A. Matin, "Dynamic behavior of MEM-mirrors for tunable-VCSELs," *Microwave and Optical Technology Letters* **39**, 203-207 (2003).

[15] D. Homentcovschi and R. N. Miles, "Viscous damping of Perforated Planar Micromechanical Structures," *Sensors and Actuators A* **119**, 544-552 (2005).

[16] Y. H. Park and K. C. Park, "High-fidelity Modeling of MEMS resonators - Part 1: Anchor loss mechanisms through substrate," *Journal of Microelectromechanical Systems* **13**, 238-247 (2004).

[17] P. Y. Kwok, M. S. Weinberg, and K. S. Breuer, "Fluid Effects in Vibrating Micromachined Structures," *J. Microelectromechanical Systems* **14**, 770-781 (2005).

[18] R. Vinokur, "Vibroacoustic Effects in MEMS," *Sound and Vibration* **37**, 22-26 (2003).

[19] T.V. Roszhart, "The Effect of Thermoelastic Internal Friction on the Q of Micromachined Silicon Resonators," Tech. Dig. Solid-State Sens. Actuator Workshop, Hilton Head, SC, pp.13-16 (1990).

[20] S. Evoy, A. Olkhovets, L. Sekaric, J. M. Parpia, H.G. Craighead, and D.W. Carr, "Temperature-Dependent Internal Friction in Silicon Nanoelectromechanical Systems," *Applied Physics Letters* **77**, 2397-2399 (2000).

[21] C. Zener, “Internal friction in solids I: theory of internal friction in reeds,” *Physical Review* **52**, 230-235 (1937).

[22] C. Zener, *Elasticity and Anelasticity of Metals*, the University of Chicago Press, Chicago 14 (1948).

[23] R. Lifshitz and M. L. Roukes, “Thermoelastic Damping in Micro- and Nanomechanical Systems,” *Physical Review B* **61**, 5600-5609 (2000).

[24] A. H. Nayfeh and M. I. Younis, “Modeling and Simulations of Thermoelastic Damping in Microplates,” *J. Micromech. Microeng.* **14**, 1711-1717 (2004).

[25] S. J. Wong, C. H. J. Fox, and S. McWilliam, “Thermoelastic Damping of the In-plane Vibration of Thin Silicon Rings,” *Journal of Sound and Vibration* **293**, 266-285 (2006).

[26] A. Duwel, J. Gorman, M. Weinstein, J. Borenstein, and P. Ward, “Experimental Study of Thermoelastic Damping in MEMS Gyros,” *Sensors and Actuators A* **103**, 70-75 (2003).

[27] Y. Sun, D. Fang, and A. K. Soh, “Thermoelastic damping in micro-beam resonators,” *International Journal of Solids and Structures* **43**, 3213-3229 (2006).

[28] B. H. Houston, D. M. Photiadis, M. H. Marcus, J. A. Bucaro, X. Liu, and J. F. Vignola, “Thermoelastic loss in microscale oscillators,” *Applied Physics Letters* **80**,1300-1302 (2002).

[29] X. Liu, J. F. Vignola, H. J. Simpson, B. R. Lemon, B. H. Houston, D. M. Photiadis, “A loss mechanism study of a very high Q silicon micromechanical oscillator,” *Journal of Applied Physics* **97**, Art No. 023524 (2005).

[30] M. J. Silver and L. D. Peterson, “Predictive Elastothermodynamic Damping in

Finite Element Models by Using a Perturbation Formulation," *AIAA Journal* **43**, 2646-2653 (2005).

[31] Y. B. Yi and M. A. Matin, "Eigenvalue Solution of Thermoelastic Damping in Beam Resonators Using a Finite Element Analysis," *ASME Journal of Vibration and Acoustics*

[32] Y. B. Yi, "Geometric Effects on Thermoelastic Damping in MEMS Resonators," *Journal of Sound and Vibration*, manuscript accepted (2007).

[33] J. P. Gorman, *Finite element analysis of thermoelastic damping in MEMS*, MS Thesis, Massachusetts Institute of Technology (Department of Materials Science and Engineering), 2002.

[34] R. Abdolvand, G. K. Ho, A. Erbil, and F. Ayazi, "Thermoelastic Damping in Trench-Refilled Polysilicon Resonators," Transducers '03 Digest of Technical Papers 1, pp.324-327 (2003)

[35] Houwen Tang, M. A. Matin and Yun-Bo Yi, "MEMS Sensors for Hearing Aid Application", *SPIE Proceedings* 6695K

[36] Lorenzo Scalise, Yanguang Yu, Guido Giulianni, Guy Plantier, and Thierry Bosch, "Self-Mixing Laser Diode Velocimetry: Application to Vibration and Velocity Measurement", IEEE Transactions on Instrumentation and Measurement, Vol.53, NO.1, February 2004.

[37] Christian Rembe, Rishi Kant, Richard S. Muller, "Optical Measurement Methods to Study Dynamic Behavior in MEMS".

[38] Ping Hua, B. Jonathan Luff, Geoffrey R. Quigley, James S. Wilkinson and Kenji Kawaguchi, " Integrated Optical Dual Mach-Zehnder Interferometer Sensor", Sensors and Actuators, B 87 (2002), 250-257.

[39] K P Zetie, S F Adams and R M Tocknell, “How Does a Mach-Zehnder Interferometer Work”, Teaching physics, IOP Science.

[40] Noge Satoru and Uno Takehiko, “Frequency Measurement of Piezoelectric Resonator Using Laser Light”, Japanese Journal of applied physics, 10.2002, vol. 41 (1), pp.3290-3294.

[41] Yi Zhang, Zhibeng Deng, Yan Li, Yanmei Han and Shulian Zhang, “An Approach for Vibration Measurement Based on Laser Frequency Splitting Technology”, Meas. Sci. Technol. 11 (2000), 1552-1556.

[42] Mitsuru Musha, Yosuke Tamura, Ken’ichi Nakagawa and Ken-ichi Ueda, “Practical Optical Frequency Measurement System Around 1.5μm Based on an Acetylene-stabilized Laser-locked Optical Frequency Comb”, Optics Communications, 272 (2007), 211-216.